Journal of Human Evolution 56 (2009) 161–174

Contents lists available at ScienceDirect

Journal of Human Evolution

journal homepage: www.elsevier.com/locate/jhevol

Allometric scaling of infraorbital surface topography in *Homo*

Scott D. Maddux [a,*], Robert G. Franciscus [a,b]

[a] Department of Anthropology, University of Iowa, Iowa City, IA 52242, USA
[b] Neuroscience Graduate Program, University of Iowa, Iowa City, IA 52242, USA

ARTICLE INFO

Article history:
Received 16 October 2007
Accepted 29 September 2008

Keywords:
Infraorbital size shape scaling
Canine fossa
Midface
Modern humans
Neandertals
Maxillary inflation

ABSTRACT

Infraorbital morphology is often included in phylogenetic and functional analyses of *Homo*. The inclusion of distinct infraorbital configurations, such as the "canine fossa" in *Homo sapiens* or the "inflated" maxilla in Neandertals, is generally based on either descriptive or qualitative assessments of this morphology, or simple linear chord and subtense measurements. However, the complex curvilinear surface of the infraorbital region has proven difficult to quantify through these traditional methods. In this study, we assess infraorbital shape and its potential allometric scaling in fossil *Homo* ($n = 18$) and recent humans ($n = 110$) with a geometric morphometric method well-suited for quantifying complex surface topographies. Our results indicate that important aspects of infraorbital shape are correlated with overall infraorbital size across *Homo*. Specifically, individuals with larger infraorbital areas tend to exhibit relatively flatter infraorbital surface topographies, taller and narrower infraorbital areas, sloped inferior orbital rims, anteroinferiorly oriented maxillary body facies, posteroinferiorly oriented maxillary processes of the zygomatic, and non-everted lateral nasal margins. In contrast, individuals with smaller infraorbital regions generally exhibit relatively depressed surface topographies, shorter and wider infraorbital areas, projecting inferior orbital rims, posteroinferiorly oriented maxillary body facies, anteroinferiorly oriented maxillary processes, and everted lateral nasal margins. These contrasts form a continuum and only appear dichotomized at the ends of the infraorbital size spectrum. In light of these results, we question the utility of incorporating traditionally polarized infraorbital morphologies in phylogenetic and functional analyses without due consideration of continuous infraorbital and facial size variation in *Homo*. We conclude that the essentially flat infraorbital surface topography of Neandertals is not unique and can be explained, in part, as a function of possessing large infraorbital regions, the ancestral condition for *Homo*. Furthermore, it appears likely that the diminutive infraorbital region of anatomically modern *Homo sapiens* is a primary derived trait, with related features such as depressed infraorbital surface topography expressed as correlated secondary characters.

© 2008 Elsevier Ltd. All rights reserved.

Introduction

The infraorbital region has long played a prominent role in the determination of systematic relationships and functional interpretation in *Homo*. This is particularly evident in the case of Neandertals and anatomically modern *Homo sapiens* (AMHS), each of which has been argued to possess derived infraorbital anatomy. The AMHS infraorbital region is generally characterized as distinctly depressed or exhibiting a "canine fossa"[1](Stringer et al., 1984; Stringer, 1985; Maureille, 1994; Lahr and Wright, 1996; Arsuaga et al., 1997, 1999; Bermúdez de Castro et al., 1997; Lieberman, 1998; Lieberman et al., 2002; Trinkaus, 2006). Conversely, the infraorbital region of Neandertals is often described as lacking a depression, and instead possessing a "puffy," inflated, or expanded infraorbital

[1] For a detailed discussion of the problematic use of the term "canine fossa" see Maureille (1994). We employ the term here as defined by Arsuaga et al. (1999): "…an extended infraorbital depression that affects most, if not the entire zygomatic process of the maxilla. We thus distinguish the canine fossa from other depressions, such as a vertical groove inferior to the infraorbital foramen (this furrow-like sulcus, which would lie lateral to the canine jugum, was called the 'sulcus maxillaris' by Weidenreich, 1943). Our definition of canine fossa is coincident with the infraorbital depression *sensu* Maureille (1994) which produces an horizontal incurvation as well as an incurvation of the zygomaticoalveolar crest."

* Corresponding author.
E-mail address: scott-maddux@uiowa.edu (S.D. Maddux).

0047-2484/$ – see front matter © 2008 Elsevier Ltd. All rights reserved.
doi:10.1016/j.jhevol.2008.10.003

morphology (Mann and Trinkaus, 1974; Heim, 1976; Smith, 1983; Stringer et al., 1984; Rak, 1986; Trinkaus, 1987, 2006; Minugh-Purvis, 1993; Maureille, 1994; Arsuaga et al., 1997, 1999; Wolpoff, 1999; Ponce de León and Zollikofer, 2001; Harvati, 2007).

The distinction between the Neandertal and the AMHS infraorbital region dates as far back as 1868, when Thomas Huxley called attention to the unusual convex configuration of the Gibraltar 1 infraorbital region in comparison to the typically concave infraorbital region of AMHS (Broca, 1869, 1878; Sollas, 1908). Huxley thus began a long standing convention of treating the convex "inflated" infraorbital region of Neandertals and the concave "canine fossa" of AMHS as dichotomized characterizations of infraorbital surface topography. However, since most researchers now accept AMHS and Neandertals as separate evolutionary lineages, it becomes important to assess whether the infraorbital morphologies of both Neandertals and AMHS are each separately derived from the morphologies present in the ancestral population from which each lineage arose from which each lineage arose (i.e. Middle Pleistocene *Homo*). This is particularly necessary as incipient expression of these distinct infraorbital features is commonly employed to infer systematic relationships within the genus *Homo*. For example, the widely accepted relationship between European *Homo heidelbergensis* and later Neandertals is based, in part, on a temporal morphocline in infraorbital flatness (Arsuaga et al., 1993, 1997; Rightmire, 1998; Bermúdez de Castro et al., 2003). Similarly, the proposed ancestral position of *Homo antecessor* to AMHS centers primarily on the presence of a canine fossa in the ATD6-69 specimen (Bermúdez de Castro et al., 1997, 1999a,b, 2003; Arsuaga et al., 1999).

An important issue in studies of infraorbital morphology has been the difficulty of assessing topographical contours across the entire infraorbital region. Sergi (1947) implemented a qualitative approach that involved visually assessing infraorbital curvature in three planes: sagittal (*incurvatio sagittalis*), coronal (*incurvatio horizontalis*), and transverse (*incurvatio inframalaris*). In his approach, specimens exhibiting curvature in all three planes (i.e., AMHS) were deemed "flexion" types, while specimens lacking curvature (i.e., Neandertals) were labeled "extension" types. Later, researchers such as Hrdlička (1952), Montagu (1960), De Villiers (1968), and Thorne (1976) implemented qualitative approaches for assessing infraorbital surface topography by sorting specimens into discrete shape categories. A number of additional infraorbital features have also been qualitatively coded (Table 1), including inferior orbital rim morphology, zygomaxillary sutural ridge prominence, zygomaticoalveolar crest curvature, malar orientation, and malar shape (Weidenreich, 1943; Sergi, 1947; De Villiers, 1968; Lahr, 1994; Lieberman, 1995; Lahr and Wright, 1996). When applied to the fossil record, these qualitative methodologies have generally supported an infraorbital dichotomy between Neandertals and AMHS, but have struggled to reach a consensus regarding the nature of the infraorbital morphologies present in Middle and Early Pleistocene *Homo* (e.g., Rak, 1986 vs. Sohn and Wolpoff, 1993). Moreover, while often informative and easily implemented, the subjective nature and proclivity for high inter- and intra-observer error in qualitative coding is widely acknowledged (Landis and Koch, 1977; Molto, 1979; De Stefano, 1983; Rösing, 1984; De Stefano et al., 1984; Espeland and Handelman, 1989).

In contrast, most metric methodologies attempting to assess size and shape of the infraorbital region have focused on measuring the maximum depth of infraorbital depression (Table 2). Many of these, such as those of Rideau (1968), Larnach and Macintosh (1970), and Lieberman et al. (2002, 2004) have involved the use of chord and subtense measures. These methods generally involve striking a chord from the landmark alare to a parallel point (relative to the Frankfurt Horizontal plane) on the zygomaxillary suture, and measuring the maximum subtense from this chord to the infraorbital surface. Alternatively, Maureille and Houët (1997a) measured the degree of the angle formed at the junction of a chord from alare to the middle of the infraorbital region (the exact midpoint between alare and the parallel point on the zygomaxillary suture) and a chord from the midpoint to the point on the zygomaxillary suture. In their analysis, AMHS generally possessed infraorbital angles of approximately 155°, while Neandertals possessed angles near or slightly greater than 180°. While these metric techniques provide a less subjective approach to assessing infraorbital depression than discrete methods, they are still considerably restricted as they assess curvature of the infraorbital region exclusively in a single transverse plane. Thus, these methods fail to

Table 1
Principal qualitative studies of infraorbital region morphology.

Terminology	Coding	Author
Canine fossa	Present/absent	Lieberman et al. (2002)
Rounding of infero-lateral margin of the orbit (RO)	Present/absent	Lahr and Wright (1996)
Infraorbital margin Malar orientation Malar shape Zygomaxillary suture ridge *Incisura malaris*	Rolled/steep Lateral/anterior Round/square Present/absent Present/absent	Lieberman (1995)
Canine fossette	Four categories of depth (absent, weak, average, strong)	Maureille (1994)
Canine fossa	Present/absent	Stringer et al. (1984)
Infraorbital fossa	Five categories of depth (absent, slight, medium, deep, very deep)	Thorne (1976)
Infraorbital excavation	Four categories of curvature in three planes: (inflated, slight moderate, marked)	De Villiers (1968)
Suborbital fossa	Three categories of depth (none, slight, marked)	Montagu (1960)
Suborbital fossa	Three categories of depth (slight, medium, pronounced)	Hrdlička (1952)
Incurvatio sagittalis *Incurvatio horizontalis* *Incurvatio inframalaris*	Present/absent	Sergi (1947)
Sulcus maxillaris	Present/absent	Weidenreich (1943)

Table 2
Principal quantitative studies assessing infraorbital region morphology.

Terminology	Measurement	Author
Canine fossa depth	Maximum subtense to the infraorbital surface from a chord between zygomaxillare and alare	Lieberman et al. (2002, 2004)
Infraorbital angle	Angle created by the vertices from alare to infra-orbitaire, and from zygomaxillaire anterior to infra-orbitaire	Maureille and Houët (1997a)
Infraorbtial fossa depth	Maximum subtense to the infraorbital surface from a chord between the midpoint of the zygomaxillary suture and a point on the lateral nasal margin "…almost at the level of the nasal floor"	Larnach & Macintosh (1970)
Suborbital fossa depth	Maximum subtense to the infraorbital surface from a chord between alare and a parallel point on zygomaxillary suture	Rideau (1968)
Suborbital fossa depth	Chord 1: basion to alare Chord 2: basion to "lateral point" (anteriormost point on zygomatic) Chord 3: basion to "medial point" (posteriormost point on infraorbital surface) Depth = ([ba-ala] + [ba-lat]/2) − (ba-med)	Birkby (1963)

assess differences in infraorbital curvature occurring superior or inferior to this axis. In addition, because these metric methods assess depth or angle exclusively at one point, they do not assess the extent of the depression along the length of the selected chord.

In recent years, many researchers have turned to geometric morphometrics to quantify anatomical morphology poorly suited for assessment with standard metric and non-metric methods. Geometric morphometric methodologies involve the collection of skeletal landmarks in three dimensional space, allowing accurate size and shape assessments of complex curvilinear structures (Rohlf, 1996; Richtsmeier et al., 2002). Informative paleoanthropological research using geometric morphometrics has been carried out on a wide array of anatomical structures with complex morphology, including the neurocranium (Bruner et al., 2004; Gunz and Harvati, 2007), mandible (Rosas and Bastir, 2004; Nicholson and Harvati, 2006), temporal bone (Harvati, 2003; Terhune et al., 2007), dentition (Martinón-Torres et al., 2006; Gómez-Robles et al., 2007), pelvis (Steyn et al., 2004; Pretorius et al., 2006), and articular joint surfaces of the hands and feet (Niewoehner, 2000, 2001, 2005, 2006; Proctor, 2005; Proctor et al., 2007).

Geometric morphometric techniques have also been extensively employed in paleoanthropological analyses of ontogenetic, static, and evolutionary allometry (e.g., Bruner and Manzi, 2001; Rosas and Bastir, 2002, 2004; Strand Viðarsdóttir et al., 2002; Mitteroecker et al., 2004; Zollikofer and Ponce De León, 2004, 2006; Ponce de León and Zollikofer, 2006; Cobb and O'Higgins, 2007). While some controversy exists over the interpretation of allometric results (see Gould, 1971; Pilbeam and Gould, 1974; Cheverud, 1982; Shea, 1985; Klingenberg, 1998; Bastir and Rosas, 2004), size has been previously recognized as a factor in several aspects of craniofacial shape (Stewart, 1977; Franciscus and Trinkaus, 1995; Lahr and Wright, 1996; Rosas, 1997; Rosas and Bastir, 2002, 2004; Franciscus, 2003). Furthermore, there is a demonstrable reduction in facial and dentognathic size in *Homo* through time (Bermúdez de Castro and Nicolás, 1995; Franciscus and Trinkaus, 1995; Wolpoff, 1999; Franciscus et al., 2007), which is particularly marked in AMHS (Lieberman et al., 2002; Trinkaus, 2003, 2006). Although a possible relationship between facial size and infraorbital surface topography has been suggested (Wolpoff et al., 1981; Trinkaus, 1987; Arsuaga et al., 1997; Pearson, 2008), a direct link between the two has yet to be quantitatively established.

The principal goals of this study are to:

1) Overcome limitations of previous studies in quantitatively assessing curvature across the entire infraorbital region by employing a well-suited geometric morphometric methodology.
2) More rigorously test the previously suggested hypothesis that infraorbital shape is correlated with infraorbital size in *Homo.*
3) Evaluate the results of these procedures in light of the various arguments regarding infraorbital surface topography in phylogenetic and adaptive contexts.

Materials and methods

Samples

The recent AMHS sample consists of 110 non-pathological crania. To maximize geographic diversity, the crania derive from six broad regions: Sub-Saharan Africa, Northeast Africa, Europe, Northeast Asia, Australia, and the Arctic Circle (Table 3). All recent crania were non-randomly selected with respect to infraorbital shape and completeness to obtain a maximum representation of intra- and inter-population variation in infraorbital shape. Selection was random with regard to other variables, including facial size. Only adult specimens as determined by complete eruption of the left and right M^3 were included in the recent comparative sample.

Table 3
Recent and fossil *Homo* samples.

Specimen	Age	Geography	Side[d]
Recent *Homo sapiens*[a]			
Arctic Circle[b] ($n = 20$)	Late Holocene	Arctic	L
Australia[b,c] ($n = 20$)	Late Holocene	Australia	L
Europe[c] ($n = 20$)	Late Holocene	Europe	L
Northeast Africa[b] ($n = 12$)	Late Holocene	Africa	L
Northeast Asia[b,c] ($n = 20$)	Late Holocene	Asia	L
Sub-Sahara Africa[c] ($n = 18$)	Late Holocene	Africa	L
Upper Paleolithic *Homo sapiens*			
Cohuna	Late Pleistocene	Australia	R
Combe-Capelle	Late Pleistocene	Europe	L
Cro-magnon 2	Late Pleistocene	Europe	R
Fish Hoek	Late Pleistocene	Africa	L
Keilor	Late Pleistocene	Australia	L
Obercassel 2	Late Pleistocene	Europe	R
Předmostí 3	Late Pleistocene	Europe	(L)[s]
Zhoukoudian Upper Cave 101	Late Pleistocene	Asia	L
Zhoukoudian Upper Cave 103	Late Pleistocene	Asia	(R)[l]
Early anatomically modern *Homo sapiens*			
Skhul 4	Late Pleistocene	Middle East	L
Late archaic *Homo*			
Jebel Irhoud 1	Middle/Late Pleist.	Africa	L
Homo neanderthalensis			
Gibraltar 1	Late Pleistocene	Europe	L
La Chapelle-aux-Saints	Late Pleistocene	Europe	(L)[l,i]
Shanidar 1	Late Pleistocene	Middle East	(R)[l]
Shanidar 5	Late Pleistocene	Middle East	(R)[l,i]
Homo heidelbergensis			
Bodo	Middle Pleistocene	Africa	L
Kabwe 1	Middle Pleistocene	Africa	L
Petralona	Middle Pleistocene	Europe	L

[a] Arctic Circle (Greenland, Siberia); Australia (Northern Territory, South Australia); Europe (Austria, British Isles, Croatia, France, Italy, Romania); Northeast Africa (Egypt); Northeast Asia (China, Japan, Korea, Mongolia); Sub-Saharan Africa (Tanzania, Botswana, Central African Republic, South Africa).
[b] National Museum of Natural History, Washington, DC.
[c] Naturhistoriches Museum, Vienna.
[d] Sides in parentheses indicate minor peripheral damage to the superior (s), lateral (l), or inferior (i) portions of the infraorbital region.

The fossil sample includes 18 specimens of Middle and Late Pleistocene *Homo* (Table 3). This fossil sample includes specimens commonly assigned to *H. neanderthalensis* and *H. heidelbergensis*. Early anatomically modern and Upper Paleolithic[2] *Homo sapiens* are additionally treated as separate fossil sub-samples. Only specimens possessing at least one essentially complete, undistorted, and matrix-free infraorbital region are included in the fossil sample. Composite specimens reconstructed from multiple individuals are also excluded. Due to the paucity of fossil specimens with perfectly preserved infraorbital regions, some specimens with minor damage to peripheral areas of the infraorbital region (see Table 3 notes) were included if surrounding anatomy permitted reasonable estimation of missing morphology. While this conservative approach unfortunately precludes the use of some fossil specimens[3], it ensures results accurately reflect credible morphology for an

[2] "Upper Paleolithic" is employed here in reference to terminal Late Pleistocene *H. sapiens* of Europe, as well as contemporaneous Australian, Asian, and African specimens associated with variously termed and generally similar lithic traditions (e.g., LSA, etc.).

[3] Specimens excluded due to distortion include Steinheim and Arago 27. Specimens excluded due to damage are numerous, including LH 18, La Ferrassie 1, Saccopastore 1, Dali, Tangshan 1, Qafzeh 6, and Qafzeh 9. Important specimens excluded due to adhering matrix include Guattari (Monte Circeo) 1, Cro-Magnon 1, and Mladec 1. Reconstructions comprised of multiple individuals (i.e., Zhoukoudian *H. erectus*) were also excluded. We were unable to access either original fossil material or casts of Sima de los Huesos 5 and Saccopastore 2 at the time of this study.

anatomical region that is frequently damaged. All fossil measurements were taken on research quality casts[4] from the National Museum of Natural History, Washington, DC, and the Paleoanthropology and Biological Anthropology cast collections housed at the University of Iowa.

Our fossil individuals most likely comprise a mixed sex group, but accurate cranial based sex determination is difficult. A recent independent corroborative study using standard osteological variables in a contemporary regionally specific sample from the Balkans (Đurić et al., 2005) documented a drop from near 100% accuracy based on aggregate pelvic traits to only ca. 70% when using aggregate skull features. Moreover, mandibular robustness was by far the single best indicator among skull features, meaning that skulls lacking mandibles would be even more difficult to sex accurately. The determination of sex, based on isolated fossil crania deriving from varying time, space, and populational/taxonomic contexts, is even more difficult due to myriad sources of potential error (Genovés, 1954; Armelagos and Van Gerven, 1980; Sládek et al., 2001; Brůžek et al., 2006). For these reasons, and because our fossil individuals in many cases lack associated mandibles or postcrania, it is imprudent to attempt sex specific analyses. In selecting our recent human comparative crania, every attempt was made to produce a sex balanced composition using standard cranial sex diagnostic markers (White, 2000; Byers, 2005), but we acknowledge the possibility of misattributions here as well. Consequently, we conduct all analyses on mixed sex-samples.

Data collection

An Immersion model 3DX Microscribe digitizer was employed to collect 3D coordinates representing a total of 20 infraorbital landmarks. To capture these 20 homologous landmarks, a standardized grid was superimposed onto each specimen (with all gridlines oriented either orthogonal or parallel to the Frankfurt Horizontal plane in which each cranium was oriented) from an LCD projector[5] equipped with leveling gauges. This grid is produced in a word processing program (Microsoft Word) as a 4×4 table, with the cells set to lock-aspect ratio to automatically maintain proportionality when the vertical and horizontal dimensions of the entire grid are manually adjusted to the boundaries of the infraorbital region. The boundaries of the superimposed grid approximate the demarcations of the hominid infraorbital plate as outlined by Rak (1986) and Trinkaus (1987). The medial border of the infraorbital region was demarcated by a vertical line passing through the lateral piriform aperture at the point alare (Fig. 1a). The lateral border was demarcated by a vertical line through the lateral orbit at ectoconchion. The superior border was demarcated by a horizontal line crossing the lower border of the orbital margin at orbitale. The inferior border was demarcated by a horizontal line passing through the metrically determined midpoint between nasospinale and prosthion. This inferior landmark was determined to most accurately represent the transition between the infraorbital region and alveolar border. Once aligned to these four infraorbital boundaries, the vertical and horizontal dimensions of each infraorbital region were represented by five equally spaced gridlines (Fig. 1b). The intersections formed by the crossing of perpendicular vertical and horizontal grid lines were digitized as homologous type III anatomical landmarks on all specimens (Bookstein, 1991). Niewoehner (2000, 2001, 2005, 2006) has previously demonstrated the utility of employing projected gridline intersections as type III landmarks on curvilinear surfaces with few standard (type I and II) skeletal landmarks. Finally, due to the shape of the zygomaticoalveolar crest, the hominid infraorbital region does not approximate the complete quadrilateral produced by the projected standardized grid. Consequently, landmarks that fail to plot on bone surface cannot be considered. When adjusted for this restriction, a total of 20 operative landmarks were obtained (Fig. 1c).

To accommodate the statistical limitations of geometric morphometric analyses in incorporating missing coordinates, landmark reconstruction was carried out on fossil specimens exhibiting minor infraorbital damage. Missing landmarks were reconstructed using the preserved morphology of surrounding areas to estimate the anatomical position of the missing landmark. Of the 18 fossil specimens, only five required the estimation of one, or at most, three landmarks (see Table 3). All measurements were taken on the left infraorbital region, except on specimens in which damage to the left infraorbital region required employment of the right side. Data from right infraorbital regions were reflected during GPA in Morphologika (version 2.5) to allow comparisons to standard left sides (O'Higgins and Jones, 2006).

Statistical analyses

Generalized Procrustes analysis (GPA) was used to superimpose the landmark configurations of all specimens using the Morphologika software program (O'Higgins and Jones, 2006). GPA superimposition translates, rotates, and scales the landmark configuration of each specimen to align it to a reference configuration (mean configuration of all specimens). Thus, GPA superimposition separates size and shape, allowing quantification of residual shape through evaluation of a specimen's deviation from the reference configuration. Concurrently, GPA superimposition preserves specimen size information as centroid size; the square root of the summed squared distances of all landmarks from the centroid (Rohlf and Slice, 1990; Bookstein, 1991; O'Higgins and Jones, 1998).

GPA superimposition was followed by principal components analysis (PCA) in the tangent plane to Kendall's shape space to summarize sample variance on ordinated orthogonal axes in order to examine most of the variability in relatively few dimensions. The shape variation represented by each principal component was determined through visualization of 3D wireframe renderings in the Morphologika software package (O'Higgins and Jones, 2006). To assess size differences in the sample, *t*-tests were conducted on infraorbital centroid size. Since the small number of specimens in each fossil sub-sample does not permit reliable comparisons between taxa, all fossil individuals were compared to the mean of the normally distributed recent AMHS sample using a modified standard two-tailed *t*-test (Sokal and Rohlf, 1981: 230). This modified *t*-test permits comparisons between measures of a single individual to a sample mean using the formula:

$$t_s = \frac{Y_1 - \overline{Y}_2}{s_2\sqrt{\frac{n_2+1}{n_2}}}$$

where Y_1 = the fossil specimen value, Y_2 = the recent AMHS sample mean, s_2 = the recent AMHS sample standard deviation, and n_2 = the recent AMHS sample size.

To test for allometric versus non-allometric effects on infraorbital shape, each individual's residual principal component shape

[4] Fossil casts used in this study were found to be accurate (< 3% difference) when compared to published original values and/or measurements taken by RGF on original specimens using a number of linear facial measurements (see Supplementary Online Material [SOM] for further details: supplementary data associated with this article can be found in the online version at doi:10.1016/j.jhevol.2008.10.003).

[5] A laser level, rather than LCD projector, was employed for grid projection on specimens housed at the Naturhistoriches Museum, Vienna (Table 3). No significant differences are attributable to the tool employed for grid projection (see repeatability discussion). The LCD projector substantially reduces time spent aligning the grid.

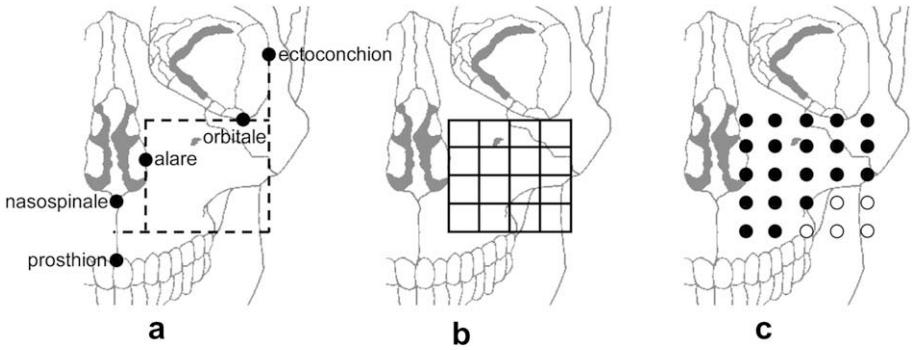

Fig. 1. (a) Landmarks used to delimit the boundaries of the infraorbital region; (b) vertical and horizontal dividing lines; and (c) 25 landmarks created by gridline intersections, with the 20 employed landmarks in black.

scores were plotted against their logged (natural log) centroid size in the statistical software package NCSS (Hintze, 2001). Linear regression was subsequently employed to test for the significance of the resulting slope coefficients, as well as to compare the correlation coefficients between these variables. To evaluate interspecific size-shape relationships, correlations and slope coefficients were calculated for all individuals in the study sample ($n = 128$). Furthermore, to minimize the effect of the disproportionately large number of AMHS individuals, correlations and slope coefficients were also calculated for AMHS sub-sample means plotted with the remaining fossil hominid individuals ($n = 16$). To evaluate intraspecific allometry, correlations and slope coefficients were also calculated for the recent AMHS individuals ($n = 110$). Unfortunately, intraspecific relationships could not be reliably assessed for *H. neanderthalensis* ($n = 4$) or *H. heidelbergensis* ($n = 3$) due to small sample sizes (see Gunz et al., 2008). Analysis of covariance (ANCOVA) was employed to compare allometric trajectories by testing for slope and intercept differences between samples. Finally, the SAS software program (9.1.3; 2000–2004) was used to conduct multivariate regression analysis using log centroid size as the independent variable and principal component shape scores as the dependent variables in all samples.

All measurements in the study were taken by one author (SDM). Intraobserver error was evaluated with ten replicates of a single recent AMHS specimen. All procedures including Frankfurt plane alignment, grid projection, landmark identification, and digitization were performed anew on each replicate. To ensure different tools employed for grid projection (laser level vs. LCD projector) did not introduce additional error, each tool was employed on five of the ten replicates. When the results of a PCA including 20 randomly selected individuals from the recent AMHS sample and ten replicates are plotted (Fig. 2), the tight clustering of the ten replicates indicates minimal intraobserver error, and high methodological repeatability (O'Higgins and Jones, 1998; Lockwood et al., 2002). The degree of overlap between replicates one through five (laser level) and six through ten (projector) indicates identical grids are produced by each tool.

Results

Principal components analysis

The first three principal components (PCs) account for nearly 70% of the total variance and quantify anatomical variation which is readily interpreted. Subsequent principal components account for substantially smaller amounts of the total variation, and accurate interpretation is difficult. Due to the large amount of cumulative variation explained, and relative ease of interpretation, only the first three principal components will be discussed.

Principal component 1 accounts for 39.6% of the total variance. This PC primarily contrasts relative infraorbital height and width, and to a lesser degree, inferior orbital rim morphology. Specimens with positive individual PC1 scores exhibit tall and narrow infraorbital areas with sloped (non-protruding) inferior orbital rims (Fig. 3a). In contrast, specimens with negative scores exhibit short and wide infraorbital areas with marked protrusion of the inferior

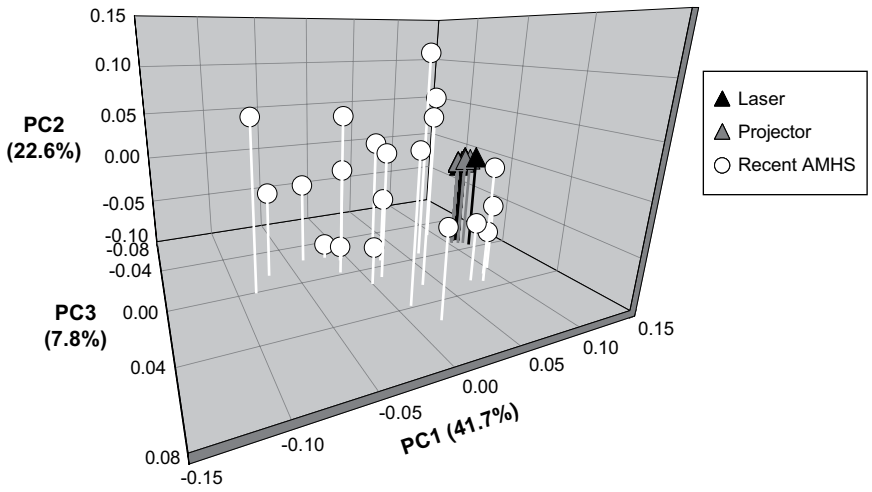

Fig. 2. 3D plot of individual PC1, PC2, and PC3 scores for the ten repeats and 20 recent AMHS individuals. Different colored triangles represent different grid projection tools. Several repeats are obscured given their propinquity.

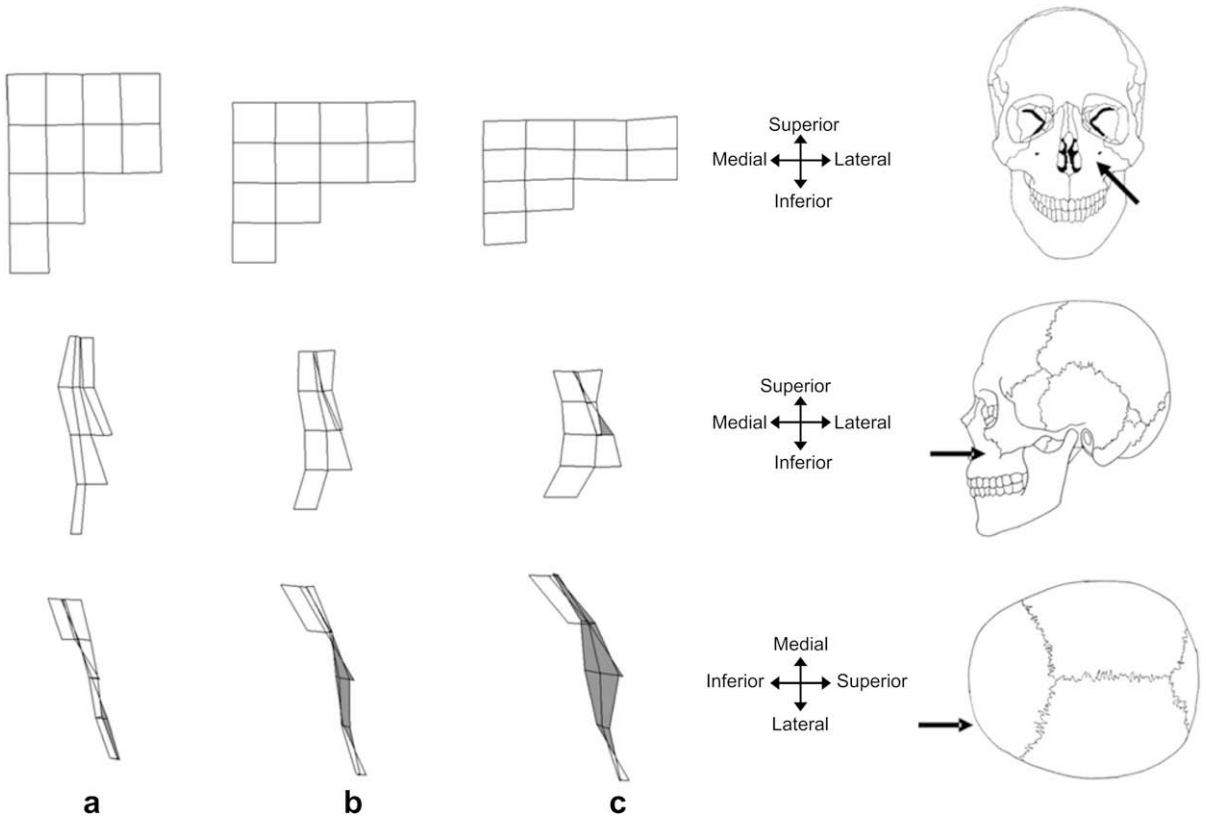

Fig. 3. Wireframe configurations of PC1 shape variation: (a) extreme positive score; (b) mean reference score; and (c) extreme negative score in anterior, lateral, and superior orientations. Anterior infraorbital surface in white, posterior surface shaded in grey. Line intersections represent digitized landmarks; lines do not represent data but are included for visualization. Crania are for orientation reference only.

orbital rim (Fig. 3c). Five fossil specimens, Combe Capelle, Fish Hoek, Keilor, Obercassel 2, and Skhul 4, display negative individual PC1 scores indicating relatively short and narrow infraorbital areas with projecting inferior orbital rims (Fig. 4). All other fossil hominids possess relatively tall and narrow infraorbital regions and sloping inferior orbital rims indicated by positive scores.

Principal component 2 accounts for 17.6% of the total variance and contrasts shape differences attributable to infraorbital depression. Individuals with positive PC2 scores exhibit less depressed or flat infraorbital surface topography (Fig. 5a), while individuals with negative scores exhibit high levels of infraorbital depression (Fig. 5c). All Neandertal and *H. heidelbergensis* specimens exhibit relatively flat infraorbital surface topographies and positive scores (Fig. 4), as do Skhul 4 and three Upper Paleolithic AMHS specimens (Fish Hoek, Obercassel 2, and Zhoukoudian PA101). All other Upper Paleolithic AMHS individuals exhibit negative PC2 scores, as does Jebel Irhoud 1, indicating relatively depressed infraorbital surfaces.

The third principal component, accounting for 10.5% of the total variance, contrasts the orientation of the maxillary body facies

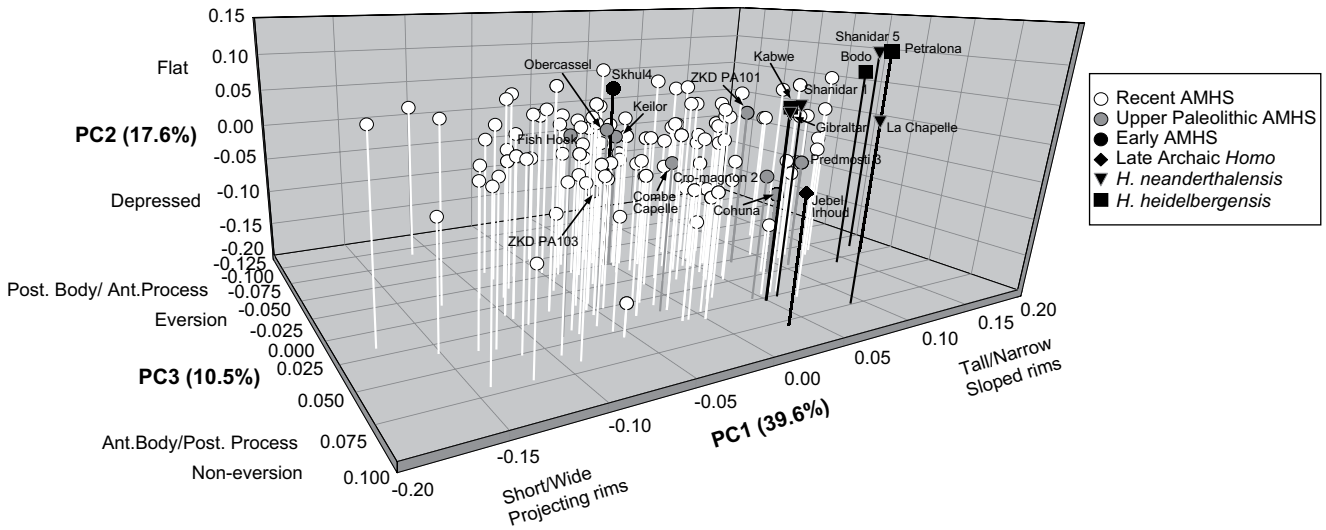

Fig. 4. 3D Plot of individual PC1, PC2, and PC3 shape scores.

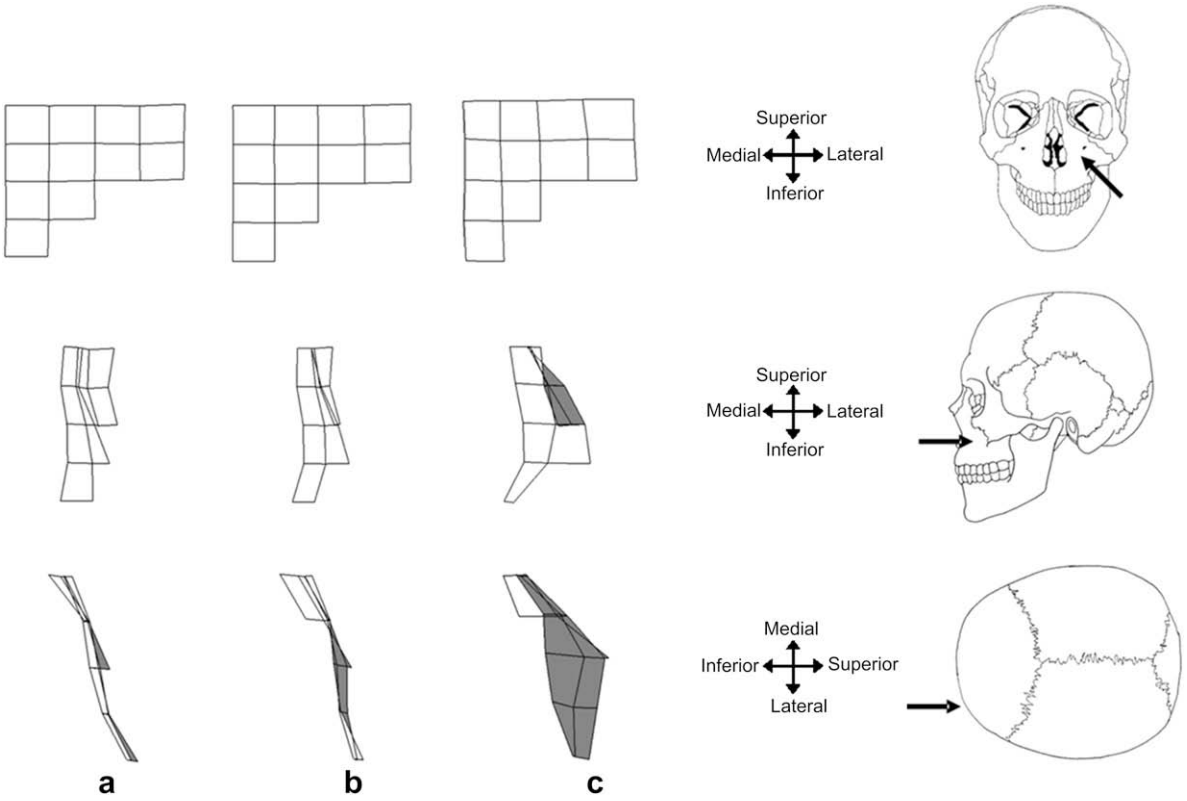

Fig. 5. Wireframe configurations of PC2 shape variation: (a) extreme positive score; (b) mean reference score; and (c) extreme negative score in anterior, lateral, and superior orientations. Anterior infraorbital surface in white, posterior surface shaded in grey. Line intersections represent digitized landmarks; lines do not represent data but are included for visualization. Crania are for orientation reference only.

(medial infraorbital region) relative to the maxillary process of the zygomatic (lateral infraorbital region). Along this axis, specimens with positive PC scores exhibit anteroinferiorly oriented maxillary body facies and posteroinferiorly oriented maxillary processes (Fig. 6a), while specimens with negative PC scores inversely exhibit posteroinferiorly oriented maxillary body facies and anteroinferiorly oriented maxillary processes (Fig. 6c). Thus, individuals at either extreme possess "twisted" infraorbital surfaces, with maxillary body facies and maxillary processes oriented in opposing directions. Individuals with intermediate scores (scores near zero) exhibit less infraorbital twisting, with maxillary body facies and processes essentially lying in the same orientation (see Fig. 6b). To a degree, the third principal component also contrasts relative anterior eversion along the medial boundary of the infraorbital region corresponding to the lateral nasal margin. Specimens with positive PC3 scores exhibit relatively non-everted lateral nasal margins at alare (Fig. 6a), while specimens with negative scores exhibit everted nasal margins (Fig. 6c). Jebel Irhoud 1 and La Chapelle exhibit strong positive PC3 scores with substantial twisting between their anteroinferiorly oriented maxillary bodies and posteroinferiorly oriented processes. Both also exhibit non-everted lateral nasal margins (Fig. 4). Gibraltar 1, Kabwe 1, Shanidar 1, Cro-magnon 2, Keilor, and Fish Hoek also demonstrate positive, albeit less extreme, PC3 scores. Among the fossils, only Combe Capelle and Skhul 4 exhibit noticeably negative scores, while all other fossil hominids display relatively intermediate scores.

Infraorbital centroid size and allometry

A large range of infraorbital size is present in the study (Fig. 7). Petralona, the largest specimen with an infraorbital centroid size of 112.6 mm, is approximately 1.8 times larger than the smallest individual in the sample, a recent AMHS individual from Egypt with a centroid size of 63.5 mm. Centroid size in the recent AMHS sample ($n = 110$) is normally distributed (both in raw and logged units) based on all standard tests for normality (e.g., Kolmogorov-Smirnov, Shapiro-Wilk, D'Agostino-Pearson omnibus). The *t*-tests on raw infraorbital centroid size indicate that all Upper Paleolithic AMHS individuals, with the exceptions of Cohuna and Předmostí 3, are not significantly different in size from the recent AMHS mean. Jebel Irhoud 1 and Skhul 4 are significantly larger than the average recent AMHS at $p < 0.05$; Cohuna, Předmostí 3, and Gibraltar 1 are significantly larger at $p < 0.005$; and the remaining Neandertal and *H. heidelbergesis* specimens are all significantly larger than the recent AMHS mean at the $p < 0.0001$ level (Table 4).

Least-squares regression of individual PC1 shape scores on log centroid size (Fig. 8a) results in a slope that is significantly different from zero ($p < 0.0001$) for all individuals in the study (Table 5). When the PC1 shape scores of the recent and Upper Paleolithic AMHS sub-sample means, rather than individuals, are regressed along with the remaining fossil individuals, the relationship is again statistically significant ($p = 0.0006$). ANCOVA results reveal no significant differences between slopes ($p = 0.7436$) or intercepts ($p = 0.8095$) between the allometric trajectories of these two interspecific samples (Table 6), indicating that the interspecific allometry among all individuals is not driven exclusively by variation within the larger AMHS sub-sample. Interestingly, however, when fossil specimens are removed from the analysis, the intraspecific association exclusively among recent AMHS individuals remains significant ($p < 0.0001$) despite the more limited size spectrum present in the recent AMHS sub-sample (Table 5). These results indicate that, both across *Homo* and within AMHS, individuals with larger infraorbital regions predictably exhibit taller and narrower infraorbital areas with more sloped inferior orbital

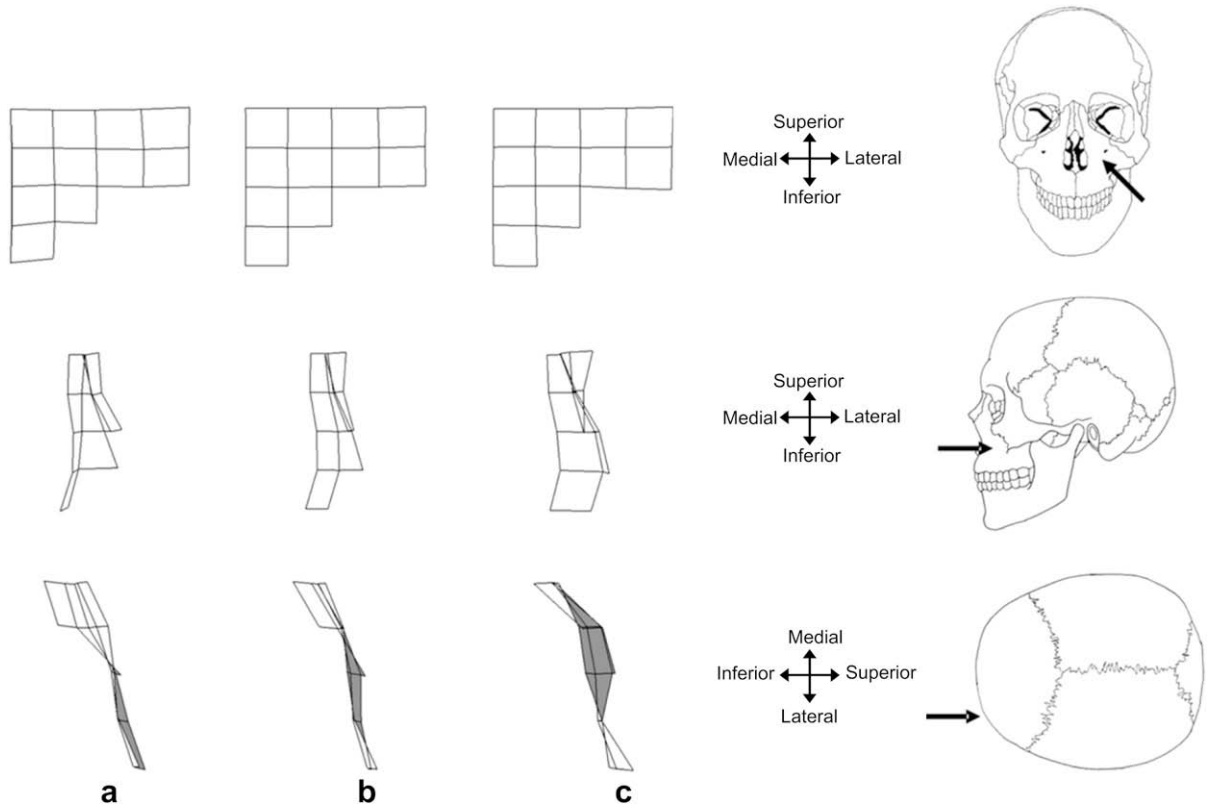

Fig. 6. Wireframe configurations of PC3 shape variation: (a) extreme positive score; (b) mean reference score; and (c) extreme negative score in anterior, lateral, and superior orientations. Anterior infraorbital surface in white, posterior surface shaded in grey. Line intersections represent digitized landmarks; lines do not represent data but are included for visualization. Crania are for orientation reference only.

rims, while individuals with smaller infraorbital regions predictably possess shorter and wider infraorbital areas with more projecting inferior orbital rims.

When individual PC2 shape scores are regressed on log centroid size, it becomes apparent that the relative degree of infraorbital depression is also correlated with infraorbital size (Fig. 8b). This size relationship is significant for all individuals in the sample ($p = 0.0004$) and for the AMHS sub-sample means and fossil hominids ($p = 0.0004$; Table 5). Again, no significant differences are present between the slopes ($p = 0.4205$) or intercepts ($p = 0.6197$)

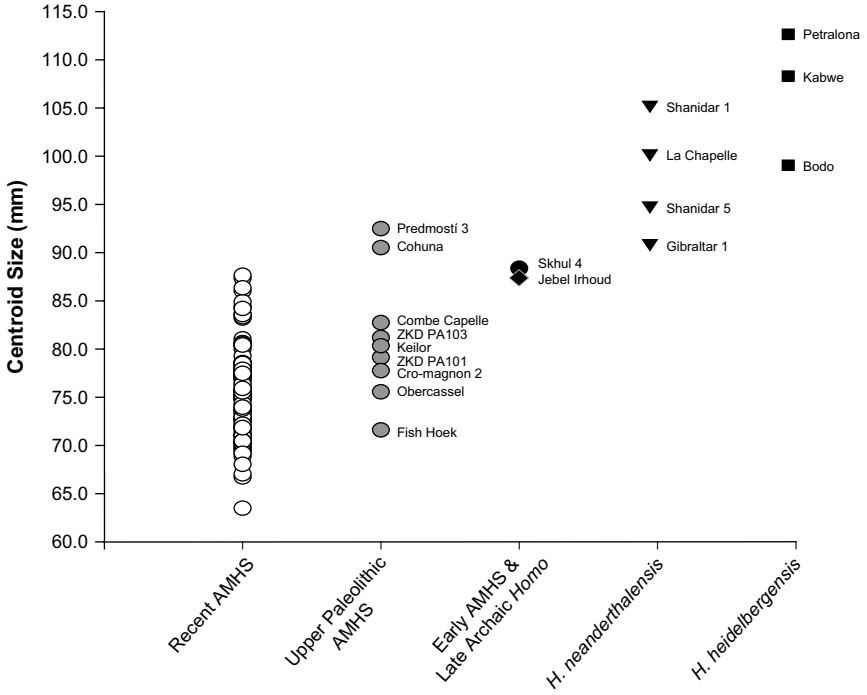

Fig. 7. Distribution of individual centroid size values.

Table 4
t-test scores comparing the centroid size of fossil individuals to the recent AMHS sample mean[a]

Specimen	t_s	p-value
Upper Paleolithic *Homo sapiens*		
Cohuna	3.086	**0.0026**
Combe-Capelle	1.462	0.1467
Cro-magnon 2	0.423	0.6733
Fish Hoek	−0.859	0.3922
Keilor	0.963	0.3377
Obercassel 2	−0.033	0.9745
Předmostí 3	3.497	**0.0007**
Zhoukoudian Upper Cave 101	0.712	0.2565
Zhoukoudian Upper Cave 103	1.141	0.4782
Early anatomically modern *Homo sapiens*		
Skhul 4	2.639	**0.0095**
Late archaic *Homo*		
Jebel Irhoud 1	2.452	**0.0158**
Homo neanderthalensis		
Gibraltar 1	3.180	**0.0019**
La Chapelle-aux-Saints	5.121	**< 0.0001**
Shanidar 1	6.173	**< 0.0001**
Shanidar 5	3.996	**< 0.0001**
Homo heidelbergensis		
Bodo	4.869	**< 0.0001**
Kabwe 1	6.799	**< 0.0001**
Petralona	7.702	**< 0.0001**

[a] p-values in bold are significant.

for the allometric trajectories of the two interspecific samples (Table 6), indicating the interspecific relationship between size and PC2 shape is not driven principally by variation among AMHS. Again, when sampled independently, a significant intraspecific relationship was found between size and PC2 shape in recent AMHS ($p = 0.0239$; Table 5). These results indicate that, both across *Homo* and within AMHS, specimens with larger infraorbital regions predictably possess relatively flatter infraorbital surfaces, while smaller specimens predictably exhibit infraorbital surfaces with more marked depression.

Regression of individual PC3 shape scores on log centroid size reveals that the relative orientations of the maxillary body facies and maxillary process, and the degree of eversion of the lateral nasal margin, are also correlated with infraorbital size (Fig. 8c). This relationship is significant among all individuals in the sample ($p = 0.0022$) and when AMHS sub-sample means and fossil hominids are assessed ($p = 0.0436$; Table 5). No significant differences are found between the slopes ($p = 0.7914$) or intercepts ($p = 0.7773$) of these two interspecific trajectories (Table 6), indicating the interspecific PC3 size-shape relationship is not merely an artifact of variation among the AMHS individuals. However, when recent AMHS individuals are sampled independently, no significant intraspecific relationship between size and PC3 shape is found ($p = 0.1547$; Table 5). Thus, across *Homo*, individuals with larger infraorbital regions predictably exhibit somewhat more anteroinferiorly oriented maxillary body facies, more posteroinferiorly oriented maxillary processes, and less everted nasal margins near alare. In contrast, individuals with small infraorbital regions predictably exhibit somewhat more posteroinferiorly oriented maxillary body facies, more anteroinferiorly oriented maxillary processes, and more everted nasal margins.

Multivariate regression employing log centroid size as the independent variable and the first three principal components as dependent variables indicates that for all individuals in the study, 44% of infraorbital shape explained collectively by PC1, PC2, and PC3 is correlated with size (Table 7). When these three principal components are regressed on log centroid size for the AMHS means and fossil individuals, the correlation between infraorbital size and

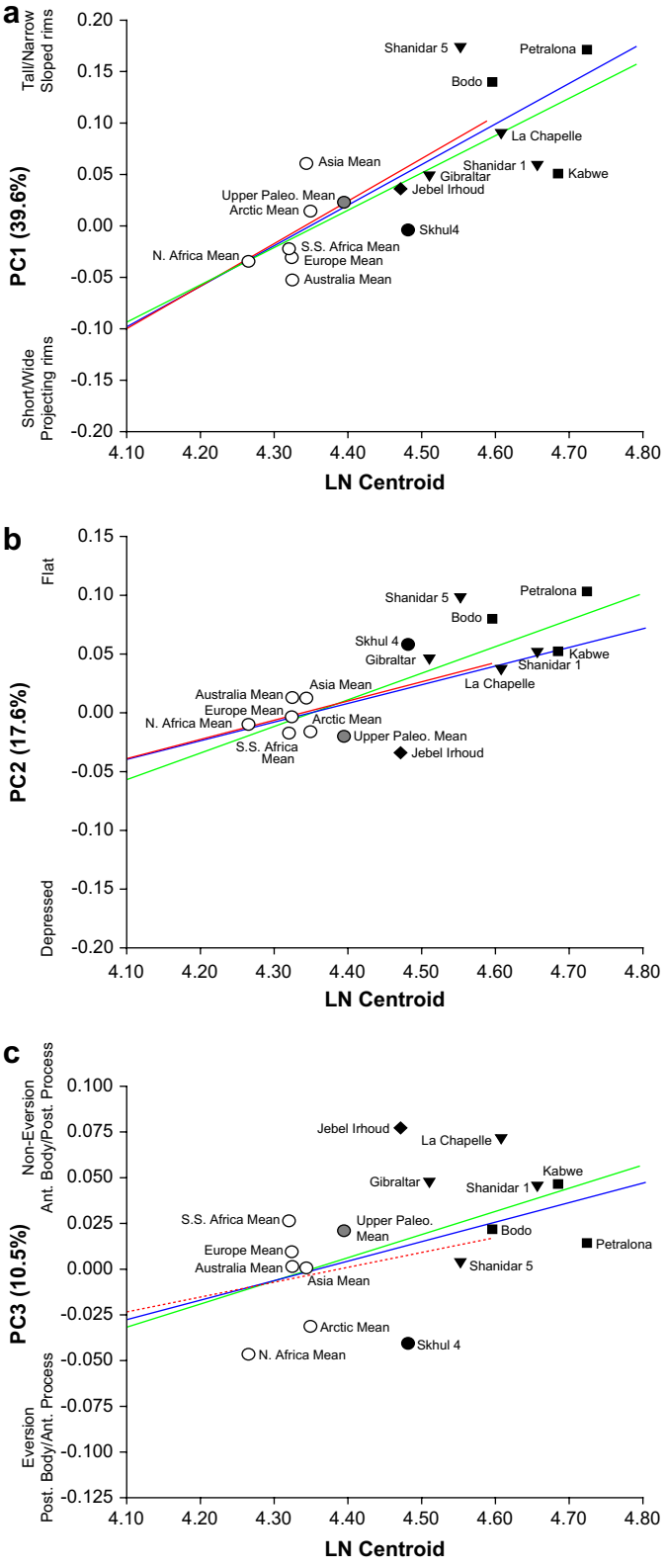

Fig. 8. Least-squares regression of (a) PC1, (b) PC2 and (c) PC3 shape scores for recent and Upper Paleolithic AMHS means and fossil hominid individuals plotted against centroid size. Symbols are the same as Fig. 4. Green regression line fitted to AMHS means and fossil hominid individuals; blue regression line fitted to all individuals; red regression line fitted to recent AMHS individuals only. Note that dashed red regression line for PC3 indicates that the slope is not significantly different from zero.

Table 5
Least squares regression results for individual PC shape scores versus $\log_e$ centroid size[a].

	n	Correlation (r)	Coefficient of determination (r^2)	Slope	p-value
PC1 (height/width; inferior rim)					
All individuals	128	0.521	0.272	0.400	**< 0.0001**
AMHS means & archaics	16	0.762	0.580	0.360	**0.0006**
Recent AMHS	110	0.387	0.150	0.429	**< 0.0001**
PC2 (depression)					
All individuals	128	0.307	0.094	0.157	**0.0004**
AMHS means & archaics	16	0.774	0.599	0.228	**0.0004**
Recent AMHS	110	0.215	0.046	0.159	**0.0239**
PC3 (twisting; eversion)					
All individuals	128	0.269	0.072	0.106	**0.0022**
AMHS means & archaics	16	0.510	0.260	0.125	**0.0436**
Recent AMHS	110	0.137	0.019	0.079	0.1547

[a] p-values in bold are significant.

shape is considerably higher, approaching 84%. In contrast, when the recent AMHS sample is analyzed, only 25% of infraorbital shape explained collectively by PC1, PC2, and PC3 is correlated with infraorbital size.

Discussion

The most salient result emerging from this study is a clear association between overall infraorbital size and shape across *Homo*, with each end of the size spectrum associated with a generally predictive set of infraorbital shape attributes (Table 8). Individuals with large infraorbital regions tend to exhibit relatively tall and narrow infraorbital areas, sloped inferior orbital rims, flat infraorbital surface topographies, anteroinferiorly oriented maxillary body facies, posteroinferiorly oriented maxillary processes, and non-everted inferolateral nasal margins. In contrast, individuals with small infraorbital regions generally possess relatively short and wide infraorbital areas, projecting inferior orbital rims, depressed surface topographies, posteroinferiorly oriented maxillary body facies, anteroinferiorly oriented maxillary processes, and everted lateral nasal margins. While the ends of the infraorbital size-shape spectrum can be contrasted, it bears repeating that these aspects of infraorbital shape are arrayed along a continuous size gradient and do not fall into truly dichotomous configurations,

Table 6
ANCOVA Results[a].

	Slope			Intercept		
	df	t_s	p-value	df	t_s	p-value
PC1 (height/width; inferior rim)						
All individuals vs. AMHS means & archaics	139	−0.328	0.7436	140	−0.241	0.8095
All individuals vs. recent AMHS	234	0.255	0.7986	235	0.077	0.9389
Recent AMHS vs. AMHS means & archaics	120	0.472	0.6380	121	0.283	0.7776
PC2 (depression)						
All individuals vs. AMHS means & archaics	139	0.808	0.4205	140	0.497	0.6197
All individuals vs. recent AMHS	234	0.029	0.9765	235	0.136	0.8920
Recent AMHS vs. AMHS means & archaics	120	−0.680	0.4976	121	−0.194	0.8466
PC3 (twisting; eversion)						
All individuals vs. AMHS means & archaics	139	0.265	0.7914	140	0.283	0.7773

[a] Note that for PC3, only one out of the three possible comparisons are made as the slope for the recent AMHS sample in this case is not significantly different from zero (see Table 5).

Table 7
Multivariate regression results for PC1, PC2, and PC3 shape scores vs $\log_e$ centroid size.

Sample	*n*	Wilks' lambda	1-Wilks' lambda[a]	p-value[b]
All individuals	128	0.562	0.438	**< 0.0001**
AMHS means and archaics	16	0.164	0.836	**< 0.0001**
Recent AMHS	110	0.749	0.251	**< 0.0001**

[a] The proportion of the generalized variance in the dependent variables (PC1, PC2, and PC3 shape scores) that is accounted for by the predictor variable ($\log_e$ centroid size).
[b] P-values in bold are significant.

as is often implicitly or explicitly argued by many researchers (e.g., Stringer et al., 1984; Rak, 1986; Arsuaga et al., 1993, 1999; Bermúdez de Castro et al., 1997; Lieberman, 1998; Smith, 2001; Tattersall and Schwartz, 2006; Harvati, 2007; Bräuer, 2008).

While the possibility of an evolutionary association between infraorbital size and shape has been suggested previously (Wolpoff et al., 1981; Trinkaus, 1987; Pearson, 2008), to the best of our knowledge, this study represents the first quantitative confirmation of infraorbital shape allometry across *Homo*. It is our contention that of the three sampling strategies employed in this study, the sample consisting of AMHS means and fossil individuals is the most appropriate for testing this hypothesis, as it minimizes the effect of disproportionately large sub-samples from a chronologically restricted time period (i.e., AMHS individuals). Consequently, the finding that 84% of the cumulative shape explained by PC1–3 in this sample is correlated with infraorbital size (Table 7) clearly indicates that size represents an important influence on infraorbital shape in later Pleistocene *Homo*.

Thus, infraorbital surface topography joins a series of other craniofacial features such as the mandibular retromolar space (Franciscus and Trinkaus, 1995; Rosas, 1997), mandibular mental foramen position (Rosas, 2001; Williams and Krovitz, 2004), nasoglabellar profile (Rosas and Bastir, 2002), internal nasal floor configuration (Franciscus, 2003), and relative piriform aperture breadth (Holton and Franciscus, 2008) demonstrating some degree of size-correlated shape change across *Homo*. Collectively, these features comprise a growing body of evidence indicating many aspects of craniofacial shape evolution in *Homo* are likely to be, at least in part, secondary allometric consequences of reduction in overall facial and dentognathic size. Consequently, there is a current need to more fully explore the mechanistic dynamics of facial size reduction through time and its relationship to developmental subunits or modules (e.g., Ackermann, 2005; Polanski and Franciscus, 2006; Rosas et al., 2006), and to more explicitly model the underlying processes driving heterochronic and heterotropic patterns in hominid evolution (e.g., Ponce de León and Zollikofer, 2006; Zollikofer and Ponce de León, 2006).

The existence of allometry in the hominid infraorbital region has important implications for the interpretation of infraorbital characters in phylogenetic contexts. The results of this study indicate that most infraorbital features array along continuous size gradients, rather than discrete polarity states. Thus, the utility of

Table 8
General summary of infraorbital size and shape allometry in *Homo*.

Shape attribute	Infraorbital size	
	Large	Small
Infraorbital area	Tall and narrow	Short and wide
Inferior orbital rim	Sloped	Projecting
Surface topography	Flat	Depressed
Maxillary body facies	Anteroinferiorly oriented	Posteroinferiorly oriented
Maxillary process	Posteroinferiorly oriented	Anteroinferiorly oriented
Lateral nasal margin	Non-everted	Everted

employing infraorbital features, such as the "canine fossa" or an "inflated" maxilla, as discrete phylogenetic traits must be called into question. While a depressed infraorbital surface, or canine fossa, is often cited as a derived feature of AMHS (Lahr and Wright, 1996; Arsuaga et al., 1997, 1999; Bermúdez de Castro et al., 1997), our results suggest that the typically depressed infraorbital morphology of AMHS may be partially explained as a function of AMHS individuals generally possessing smaller faces than those of middle Pleistocene hominids. In other words, it may be the significantly reduced facial size and diminutive infraorbital region of AMHS that is derived, with depressed infraorbital morphology expressed as a correlated secondary character. Accordingly, smaller infraorbital size may also account for the reportedly more "modern" appearing infraorbital regions of specimens such as LH-18 (Smith et al., 1989), Steinheim (Howell, 1951), Tangshan 1 (Wang and Tobias, 2000; Wu et al., 2005), Gran Dolina ATD6-69 (Bermúdez de Castro et al., 1997; Arsuaga et al., 1999), and Liang Bua 1 (Jacob et al., 2006; Hershkovitz et al., 2007); although allowances for deformation (Steinheim), subadult status (ATD6-69), and possible pathology (Liang Bua 1) must also be considered.

Our results also question the derived status of the "inflated" or "puffy" maxilla, seen by many workers (e.g., Stringer et al. 1984; Rak, 1986; Arsuaga et al., 1997; Arsuaga et al., 1999) as a Neandertal apomorphy, and its various biomechanical and climatic interpretations (Heim, 1978; Smith, 1983; Demes, 1987; Trinkaus, 1987; Wolpoff, 1999) among Neandertals in adaptive contexts. The overlap of Neandertal, *H. heidelbergensis,* and large-faced AMHS PC scores, especially PC2 scores (Fig. 4), indicates that Neandertals do not possess uniquely inflated infraorbital surface topographies. Rather, the essentially flat infraorbital region of Neandertals can be explained primarily as a function of possessing large infraorbital regions, similar in size to *H. heidelbergensis,* but significantly larger than the average recent AMHS. Thus, while features peripheral to the infraorbital region, such as the superior nasal and zygomatic regions along with a somewhat more parasagittaly oriented infraorbital plane, may represent derived Neandertal characteristics (Rak, 1986; Trinkaus, 1987; Maureille and Houët, 1997b; Franciscus, 1999), infraorbital surface topography by itself does not.

Additionally, it is interesting to note that the greatest degree of infraorbital variation across *Homo* is not principally related to infraorbital depression. The first principal component in our study, which contrasts relative height and width of the infraorbital region along with infraorbital margin projection, accounts for approximately 40% of total infraorbital shape variation, more than twice the amount of variation accounted for by the second principal component which contrasts infraorbital depression. This is surprising, as the majority of previous studies of the infraorbital region, both qualitative and quantitative, have focused on depression rather than infraorbital width to height relationships. While width of the infraorbital region was considered in Rideau's (1968) study of geographic variation in recent AMHS infraorbital depression, this study lacked data regarding vertical dimensions of the infraorbital region and consequently lacked height and width comparisons.

Inferior orbital rim morphology, the second aspect of the first principal component, was discussed by Sollas in 1908, and since then other researchers (e.g., Weidenreich 1943, Frayer et al., 1993; Lahr, 1994; Lieberman, 1995; Lahr and Wright, 1996) have qualitatively coded inferior orbital rim morphology. However, we are unaware of any previous quantitative assessment of this particular infraorbital feature. Future research may demonstrate that projecting inferior orbital rims in hominids with smaller infraorbital regions are principally related to spatial constraints of structures such as the orbital floor, maxillary sinus, or even muscles of facial expression. Regardless, it is likely that the presence of a projecting inferior orbital rim accentuates the visual perception of infraorbital depression in individuals with small infraorbital regions, while a sloped inferior orbital rim may exaggerate the "inflated" appearance of relatively flat infraorbital regions in individuals with larger infraorbital regions.

The infraorbital morphology contrasted in our third principal component has also received some attention in previous infraorbital studies. Some researchers (Rak, 1986; Sohn and Wolpoff, 1993; Bermúdez de Castro et al., 1997; Arsuaga et al., 1999) have discussed the posteroinferior orientation of the infraorbital surface in AMHS relative to the anteroinferior orientation observed in earlier hominids, but we are unaware of any previous research exploring the orientation of the maxillary body facies relative to the orientation of the maxillary process of the zygomatic. In conjunction with a projecting inferior orbital rim, the posteroinferiorly oriented maxillary body facies and anteroinferiorly oriented maxillary process likely intensify the appearance of concave or depressed infraorbital morphology in individuals with smaller infraorbital regions. Conversely, the anteroinferiorly oriented maxillary body facies and posteroinferiorly oriented process likely enhance the visual appearance of flat or convex infraorbital surface topography in individuals with larger infraorbital regions.

Additionally, PC3 also contrasts variation in anterior eversion of the lateral nasal margin near alare. Arsuaga et al. (1999) have previously suggested AMHS to be characterized by a derived two-plane infraorbital configuration in which the lateral nasal margin (i.e., medial infraorbital region) is everted anteriorly (parasagittally), while the rest of the maxillary body facies (i.e., the lateral infraorbital region) lies predominantly in the coronal plane (see also Franciscus, 2002; Franciscus and Vlček, 2006). This "flexed" configuration of AMHS can be contrasted with the premodern "uniplanar" condition in which the entire infraorbital surface lies essentially in a single plane. In our study, lateral nasal margin eversion is correlated with infraorbital centroid size across *Homo*. However, this correlation is not evident within the AMHS sample, suggesting that most recent AMHS individuals possess at least some degree of lateral nasal margin eversion. Thus, this result appears consistent with Arsuaga et al.'s (1999) suggestion of a characteristic two-plane configuration in AMHS.

Our discussion to this point has mostly emphasized issues relevant across genus *Homo* (i.e., interspecifically). Unfortunately, the small number of Neandertal and *H. heidelbergensis* individuals in this study precludes the ability to construct robust intraspecific allometric trajectories for all taxa (see Gunz et al., 2008). However, given the similarity between the recent AMHS intraspecific slope and the two interspecific slopes for both PC1 and PC2 (see Fig. 8 and Table 6), the possibility that common infraorbital allometric trajectories may characterize *Homo* both inter- and intraspecifically cannot be rejected. Moreover, it has been noted that late Neandertal maxillary remains from Vindija (Vi 259) and Kůlna Cave, while fragmentary and incomplete, appear to show shallow "canine fossae" along with clearly reduced overall facial dimensions relative to earlier Neandertals (Wolpoff et al., 1981; Smith et al., 1989). These observations appear consistent with similar allometric trajectories in infraorbital depression among both AMHS and Neandertals. Conversely, the lack of a significant correlation between centroid size and PC3 shape in the recent AMHS sample (Fig. 8 and Table 5), may indicate distinct differences in the relationship between size and PC3 shape within each species of *Homo*.

The AMHS intraspecific results for the first two principal components confirm the importance of the sampling strategy we employed for the recent humans. By incorporating the fullest possible range of infraorbital shape, we assured the possibility that any potential association with size (which was ignored in the selection process) would be elucidated. A purely random selection process in which infraorbital shape variation was ignored would almost certainly not have sampled the full range of both infraorbital shape and size across which allometric scaling manifests.

Finally, it is important to acknowledge that this study assesses infraorbital surface topography without regard to relative position and orientation to other facial structures. Several researchers, most notably Maureille and Houët (1997b), have argued orientation of the infraorbital region to be of greater phylogenetic importance than surface morphology. Other researchers, such as Smith (1983), Rak (1986), Demes (1987), and Trinkaus (1987) have suggested infraorbital orientation may have important biomechanical implications for stress dissipation. While our study does not consider infraorbital orientation, we contend that the longstanding and continued use of strictly topographical features such as the "canine fossa" and "inflated" maxilla in paleoanthropological discussions, without regards to infraorbital orientation, has warranted this exclusively topographical exploration of the infraorbital region.

Acknowledgements

We are indebted to the following individuals for providing access to skeletal and cast material under their care: M. Teschler-Nicola, K. Wiltschke-Schrotta, M. Berner, D. Hunt, and J. Clark. We thank S. Miller, D. Proctor, C. Terhune, and especially N. Holton for helpful comments regarding analytical aspects of this study. We also wish to thank B. Maureille, F. Smith, K. Harvati, J. Polanski, and H. Marsh for insightful discussions. S. Antón and four anonymous reviewers also provided constructive comments which improved this manuscript. We additionally thank J. Rodgers for aid with the arrangement of several figures and C. Franciscus for aid in SAS modeling. This work was supported by grants from UISG and the UI Department of Anthropology.

Supplementary data

Supplementary data associated with this article can be found in the online version, at doi:10.1016/j.jevol.2008.10.003.

References

Ackermann, R.R., 2005. Ontogenetic integration of the hominoid face. J. Hum. Evol. 48, 175–197.
Armelagos, G.J., Van Gerven, D.P., 1980. Sexual dimorphism and human evolution: an overview. J. Hum. Evol. 9, 437–446.
Arsuaga, J.L., Martínez, I., Gracia, A., Carretero, J.M., Carbonell, E., 1993. Three new human skulls from the Sima de los Huesos middle Pleistocene site in Sierra de Atapuerca, Spain. Nature 362, 534–537.
Arsuaga, J.L., Martínez, I., Gracia, A., Lorenzo, C., 1997. The Sima de Los Huesos crania (Sierra de Atapuerca, Spain). A comparitive study. J. Hum. Evol. 33, 219–281.
Arsuaga, J.L., Martínez, I., Lorenzo, C., Gracia, A., 1999. The human cranial remains from Gran Dolina Lower Pleistocene Site (Seirra de Atapuerca, Spain). J. Hum. Evol. 37, 431–457.
Bastir, M., Rosas, A., 2004. Geometric morphometrics in paleoanthropology: mandibular shape variation, allometry, and the evolution of modern human skull morphology. In: Elewa, A.M.T. (Ed.), Morphometrics: Applications in Biology and Paleontology. Springer-Verlag, Heidelberg, pp. 231–244.
Bermúdez de Castro, J.M., Arsuaga, J.L., Carbonell, E., Rosas, A., Martinez, I., Mosquera, M., 1997. A Hominid from the Lower Pleistocene of Atapuerca, Spain: possible ancestor to Neandertals and modern humans. Science 276, 1392–1395.
Bermúdez de Castro, J.M., Carbonell, E., Cáceres, I., Díez, J.C., Fernández-Jalvo, Y., Mosquera, M., Ollé, A., Rodríguez, J., Rodríguez, X.P., Rosas, A., 1999a. The TD6 (Aurora stratum) hominid site. Final remarks and new questions. J. Hum. Evol. 37, 695–700.
Bermúdez de Castro, J.M., Martinon-Torres, M., Sarmiento, S., Lozano, M., 2003. Gran Dolina-TD6 versus Sima de los Huesos dental samples from Atapuerca: evidence of discontinuity in the European Pleistocene population? J. Archaeol. Sci. 30, 1421–1428.
Bermúdez de Castro, J.M., Nicolás, E., 1995. Posterior dental size reduction in hominids: the Atapuerca evidence. Am. J. Phys. Anthropol. 96, 335–356.
Bermúdez de Castro, J.M., Rosas, A., Nicolás, M.E., 1999b. Dental remains from Atapuerca-TD6 (Gran Dolina site, Burgos, Spain). J. Hum. Evol. 37, 523–566.
Birkby, W.H., 1963. Subjective and metrical depth of the suborbital fossa. Masters Thesis, University of Kansas, Lawrence.
Bookstein, F.L., 1991. Morphometric Tools for Landmark Data: Geometry and Biology. Cambridge University Press, Cambridge.
Bräuer, G., 2008. The origin of modern anatomy: by speciation or intraspecific evolution? Evol. Anthropol. 17, 22–37.
Broca, P., 1869. Remarques sur les ossements des cavernes de Gibraltar 1. Bull. Mém. Soc. Anthropol. Paris. 4, 146–158.
Broca, P., 1878. Translation of the greater part of the address delivered by M. Broca, president, at the opening meeting of the French Association for the Advancement of the Sciences, at the Havre Congress, 1877. J. Anthropol. Inst. Great. Brit. Ireland 7, 187–200.
Bruner, E., Manzi, G., 2001. Allometric analysis of the skull in *Pan* and *Gorilla* by geometric morphometrics. Riv. Antropo. (Roma) 79, 45–52.
Bruner, E., Saracino, B., Ricci, F., Tafuri, M., Passarello, P., Manzi, G., 2004. Midsagittal cranial shape variation in the genus *Homo* by geometric morphometrics. Coll. Antropol. 28, 99–112.
Brůžek, J., Franciscus, R.G., Novotný, V., Trinkaus, E., 2006. The assessment of sex. In: Trinkaus, E., Svoboda, J. (Eds.), Early Modern Human Evolution in Central Europe: The People of Dolni Vestonice and Pavlov. Oxford University Press, London, pp. 46–62.
Byers, S., 2005. Introduction to Forensic Anthropology: A Textbook, second ed. Allyn & Bacon, Boston.
Cheverud, J.M., 1982. Relationships among ontogenetic, static, and evolutionary allometry. Am. J. Phys. Anthropol. 59, 139–149.
Cobb, S.N., O'Higgins, P., 2007. The ontogeny of sexual dimorphism in the facial skeleton of the African apes. J. Hum. Evol. 53, 176–190.
Demes, B., 1987. Another look at an old face: biomechanics of the Neandertal facial skeleton reconsidered. J. Hum. Evol. 16, 297–303.
De Stefano, G.F., 1983. Inter- and intra-observer variability in the interpretation of the "discrete" characters of the skull. J. Hum. Evol. 12, 690.
De Stefano, G.F., Hauser, G., Guidotti, A., Rossi, S., Gualdi Russo, E., Brasili Gualandi, P., 1984. Reflections on interobserver differences in scoring nonmetric cranial traits (with practical examples). J. Hum. Evol. 13, 349–355.
De Villiers, H., 1968. The Skull of the South African Negro. A Biometrical and Morphometrical Study. Witwatersrand University Press, Johannesburg.
Đurić, M., Zoran Rakoćević, Z., Đonić, D., 2005. The reliability of sex determination of skeletons from forensic context in the Balkans. Forensic. Sci. Int. 147, 159–164.
Espeland, M.A., Handelman, S.L., 1989. Using latent class models to characterize and assess relative error in discrete measurements. Biometrics 45, 587–599.
Franciscus, R.G., 1999. Neandertal nasal structures and upper respiratory tract "specialization". Proc. Natl. Acad. Sci. 96, 1805–1809.
Franciscus, R.G., 2002. The midfacial morphology. In: Zilhão, J., Trinkaus, E. (Eds.), Portrait of the Artist as a Child. The Gravettian Human Skeleton from the Abrigo do Lagar Velho and its Archeological Context. Trabalhos de Arqueologia, vol. 22. Instituto Português de Arqueologia, Lisboa, pp. 297–311.
Franciscus, R.G., 2003. Internal nasal floor configuration in *Homo* with special reference to the evolution of Neandertal facial form. J. Hum. Evol. 44, 701–729.
Franciscus, R.G., Holton, N.E., Maddux, S.D., Marsh, H.E., Ciochon, R.L., 2007. Temporal and geographic patterning of mandibular corpus dimensions in *Homo* using Mantel tests. Am. J. Phys. Anthropol. 42S, 110.
Franciscus, R.G., Trinkaus, E., 1995. Determinants of retromolar space presence in Pleistocene *Homo* mandibles. J. Hum. Evol. 28, 577–595.
Franciscus, R.G., Vlček, E., 2006. The cranial remains. In: Trinkaus, E., Svoboda, J. (Eds.), Early Modern Human Evolution in Central Europe: The People of Dolní Věstonice and Pavlov. Oxford University Press, London, pp. 63–152.
Frayer, D.W., Wolpoff, M.H., Thorne, A.G., Smith, F.H., Pope, G.G., 1993. Theories of modern human origins: the paleontological test. Am. Anthropol. 95, 14–50.
Genovés, S., 1954. The problem of the sex of certain fossil hominids, with special reference to the Neandertal skeletons from Spy. J.R. Anthropol. Inst. 84, 131–144.
Gómez-Robles, A., Martinón-Torres, M., Bermúdez de Castro, J.M., Margvelashvili, A., Bastir, M., Arsuaga, J.L., Pérez-Pérez, A., Estebaranz, F., Martínez, L.M., 2007. A geometric morphometric analysis of hominid upper first molar shape. J. Hum. Evol. 53, 272–285.
Gould, S.J., 1971. Geometric similarity in allometric growth: a contribution to the problem of scaling in the evolution of size. Am. Nat. 105, 113–136.
Gunz, P., Bookstein, F.L., Weber, G.W., Hublin, J.J., 2008. Why small fossil samples are such a big problem. Am. J. Phys. Anthropol. 46S, 110–111.
Gunz, P., Harvati, K., 2007. The Neanderthal "chignon": variation, integration, and homology. J. Hum. Evol. 52, 262–274.
Harvati, K., 2003. Quantitative analysis of Neanderthal temporal bone morphology using three-dimensional geometric morphometrics. Am. J. Phys. Anthropol. 120, 323–328.
Harvati, K., 2007. Neanderthals and their contemporaries. In: Henke, W., Tattersall, I. (Eds.), Handbook of Paleoanthropology, vol. 3. Springer, New York, pp. 1718–1748.
Heim, J.L., 1976. Les hommes fossiles de La Ferrassie I: le gisement, les squelettes adultes (crane et squelette du tronc). Arch. Inst. Paleóntol. Humaine 35, 1–131.
Heim, J.L., 1978. Contribution du massif facial a la morphogenese du crane Neanderthalien. In: Piveteau, J. (Ed.), Les origines humaines et les epoques de l'intelligence. Masson, Paris, pp. 183–215.
Hershkovitz, I., Kornreich, L., Laron, Z., 2007. Comparative skeletal features between *Homo floresiensis* and patients with primary growth hormone insensitivity (Laron syndrome). Am. J. Phys. Anthropol. 134, 198–208.
Hintze, J., 2001. NCSS and PASS. Number Cruncher Statistical Systems. Kaysville, Utah.
Holton, N.E., Franciscus, R.G., 2008. The paradox of a wide nasal aperture in cold-adapted Neandertals: a causal assessment. J. Hum. Evol. 55, 942–951.
Howell, F.C., 1951. The place of Neanderthal man in human evolution. Am. J. Phys. Anthropol. 9, 379–416.
Hrdlička, A., 1952. Practical anthropometry, fourth ed. In: Stewart, T.D. (Ed.). The Wistar Institute of Anatomy and Biology, Philadelphia.

Jacob, T., Indriati, E., Soejono, R.P., Hsü, K., Frayer, D.W., Eckhardt, R.B., Kuperavage, A.J., Thorne, A., Henneberg, M., 2006. Pygmoid Australomelanesian *Homo sapiens* skeletal remains from Liang Bua, Flores: population affinities and pathological abnormalities. Proc. Nat. Acad. Sci. 103, 13421–13426.

Klingenberg, C.P., 1998. Heterochrony and allometry: the analysis of evolutionary change in ontogeny. Biol. Rev. 73, 79–123.

Lahr, M.M., 1994. The multiregional model of modern human origins: a reassessment of its morphological basis. J. Hum. Evol. 26, 23–56.

Lahr, M.M., Wright, R.V.S., 1996. The question of robusticity and the relationship between cranial size and shape in *Homo sapiens*. J. Hum. Evol. 31, 157–191.

Landis, J.R., Koch, G.G., 1977. The measurement of observer agreement for categorical data. Biometrics 33, 159–174.

Larnach, S.L., Macintosh, N.W.G., 1970. The craniology of the aborigines of Queensland. Oceania Monographs, 15.

Lieberman, D.E., 1995. Testing hypotheses about recent human evolution from skulls: integrating morphology, function, development, and phylogeny. Curr. Anthropol. 36, 159–197.

Lieberman, D.E., 1998. Sphenoid shortening and the evolution of modern human cranial shape. Nature 393, 158–162.

Lieberman, D.E., Krovitz, G.E., McBratney-Owen, B., 2004. Testing hypotheses about tinkering in the fossil record: the case of the human skull. J. Exp. Zool. B. Mol. Dev. Evol. 302, 284–301.

Lieberman, D.E., McBratney, B., Kovitz, G.E., 2002. The evolution and development of cranial form in *Homo sapiens*. Proc. Nat. Acad. Sci. 99, 1134–1139.

Lockwood, C.A., Lynch, J.M., Kimbel, W.H., 2002. Quantifying temporal bone morphology of great apes and humans: an approach using geometric morphometrics. J. Anat. 201, 447–464.

Mann, A.E., Trinkaus, E., 1974. Neandertal and Neandertal-like fossils from the Upper Pleistocene. Yearb. Phys. Anthropol. 17, 169–193.

Martinón-Torres, M., Bastir, M., Bermúdez de Castro, J.M., Gómez, A., Sarmiento, S., Muela, A., Arsuaga, J.L., 2006. Hominid lower second premolar morphology: evolutionary inferences through geometric morphometric analysis. J. Hum. Evol. 50, 523–533.

Maureille, B., 1994. La face chez *Homo erectus* et *Homo sapiens*: recherche sur la variabilité morphologique et métrique. Ph.D. Dissertation, University of Bordeaux I.

Maureille, B., Houët, F., 1997a. Nouvelles données sur charactèristiques derivées du masif facial superieur des Neandertaliens. Anthropol. Prehistorie 108, 89–98.

Maureille, B., Houët, F., 1997b. L'orientation spatiale des surfaces infra-orbitaires maxillozygomatiques chez *Homo sapiens*: une clef de la compréhension de la face neandertalienne. Biom. Hum. Anthropol. 15, 75–80.

Minugh-Purvis, N., 1993. Reexamination of the immature hominid maxilla from Tangier, Morocco. Am. J. Phys. Anthropol. 92, 449–461.

Mitteroecker, P., Gunz, P., Bernhard, M., Schaefer, K., Bookstein, F.L., 2004. Comparison of cranial ontogenetic trajectories among great apes and humans. J. Hum. Evol. 46, 679–698.

Molto, J.E., 1979. The assessment and meaning of intraobserver error in population studies based on discontinuous cranial traits. Am. J. Phys. Anthropol. 51, 333–344.

Montagu, M.F., 1960. A Handbook of Anthropometry. Charles C. Thomas Publisher, Springfield.

Nicholson, E., Harvati, K., 2006. Quantitative analysis of human mandibular shape using three-dimensional geometric morphometrics. Am. J. Phys. Anthropol. 131, 368–383.

Niewoehner, W.A., 2000. The functional anatomy of late Pleistocene and recent human carpometacarpal and metacarpophalangeal articulations. PhD. Dissertation, University of New Mexico.

Niewoehner, W.A., 2001. Behavioral inferences from the Skhul/Qafzeh early modern human hand remains. Proc. Natl. Acad. Sci. 98, 2979–2984.

Niewoehner, W.A., 2005. A geometric morphometric analysis of Late Pleistocene human metacarpal 1 base shape. In: Slice, D. (Ed.), Modern Morphometrics in Physical Anthropology. Kluwer Academic/Plenum, New York, pp. 285–298.

Niewoehner, W.A., 2006. Neanderthal hands in their proper perspective. In: Harvati, K., Harrison, T. (Eds.), Neanderthals Revisted: New Approaches and Perspectives. Springer, Dordrecht, pp. 157–190.

O'Higgins, P., Jones, N., 1998. Facial growth in *Cercocebus torquatus*: an application of three-dimensional geometric morphometric techniques to the study of morphological variation. J. Anat. 193, 251–272.

O'Higgins, P., Jones, N., 2006. Tools for Statistical Shape Analysis. Available from:. Hull York Medical School http://www.york.ac.uk/res/fme/resources/software.htm.

Pearson, O.M., 2008. Statistical and biological definitions of "anatomically modern" humans: suggestions for a unified approach to modern morphology. Evol. Anthropol. 17, 38–48.

Pilbeam, D., Gould, S.J., 1974. Size and scaling in human evolution. Science 186, 892–901.

Polanski, J.M., Franciscus, R.G., 2006. Patterns of craniofacial integration in extant *Homo, Pan*, and *Gorilla*. Am. J. Phys. Anthropol. 131, 38–49.

Ponce de León, M.S., Zollikofer, C.P.E., 2001. Neanderthal cranial ontogeny and its implications for late hominid diversity. Nature 412, 534–538.

Ponce de León, M.S., Zollikofer, C.P.E., 2006. Neanderthals and modern humans—chimps and bonobos: similarities and differences in development and evolution. In: Harvati, K., Harrison, T. (Eds.), Neanderthals Revisited: New Approaches and Perspectives. Springer, Dordrecht, pp. 71–88.

Pretorius, E., Steyn, M., Scholtz, Y., 2006. Investigation into the usability of geometric morphometric analysis in assessment of sexual dimorphism. Am. J. Phys. Anthropol. 129, 64–70.

Proctor, D.J., 2005, Morphometrics and multi-landmark depth analysis of the proximal hallucal metatarsal articular surface in hominoid. Masters Thesis, Florida Atlantic University.

Proctor, D.J., Broadfield, D., Proctor, K., 2007. Quantitative three-dimensional shape analysis of the proximal hallucial metatarsal articular surface in *Homo, Pan, Gorilla, and Hylobates*. Am. J. Phys. Anthropol. 137, 216–224.

Rak, Y., 1986. The Neanderthal: a new look at an old face. J. Hum. Evol. 15, 151–164.

Richtsmeier, J.T., DeLeon, V.B., Lele, S.R., 2002. The promise of geometric morphometrics. Yearb. Phys. Anthropol. 45, 63–91.

Rideau, Y., 1968. Etude anthropometrique de la fosse sous-orbitaire. Bull. Mem. Soc. Anthropol. Paris. 12, 317–329.

Rightmire, G.P., 1998. Human evolution in the middle Pleistocene: the role of *Homo heidelbergensis*. Evol. Anthropol. 6, 218–227.

Rohlf, F.J., 1996. Morphometric spaces, shape components and the effects of linear transformations. In: Marcus, L.F. (Ed.), Advances in Morphometrics. Plenum Press, New York, pp. 117–128.

Rohlf, F.J., Slice, D., 1990. Extensions of the Procrustes method for the optimal superimposition of landmarks. Syst. Zool. 39, 40–59.

Rosas, A., 1997. A gradient of size and shape for the Atapuerca sample and middle Pleistocene hominid variability. J. Hum. Evol. 33, 319–331.

Rosas, A., 2001. Occurrence of Neanderthal features in mandibles from the Atapuerca-SH site. Am. J. Phys. Anthropol. 114, 74–91.

Rosas, A., Bastir, M., 2002. Thin-plate spline analysis of allometry and sexual dimorphism in the human craniofacial complex. Am. J. Phys. Anthropol. 117, 236–245.

Rosas, A., Bastir, M., 2004. Geometric morphometric analysis of allometric variation in the mandibular morphology of the hominids of Atapuerca, Sima de los Huesos site. Anat. Rec. A. Discov. Mol. Cell. Evol. Biol. 278, 551–560.

Rosas, A., Bastir, M., Martínez-Maza, C., García-Tabernero, A., Lalueze-Fox, C., 2006. Inquiries into Neanderthal craniofacial development and evolution: "accretion" versus "organismic" models. In: Harvati, K., Harrison, T. (Eds.), Neanderthals Revisited: New Approaches and Perspectives. Springer, Dordrecht, pp. 37–69.

Rösing, F.W., 1984. Discreta of the human skeleton: a critical review. J. Hum. Evol. 13, 319–323.

SAS Institute Inc. 2000–2004. SAS 9.1.3, Cary, NC.

Sergi, S., 1947. Sulla morfologia della "facies anterior corporis maxillae" nei paleanthroi di Saccopastore e del Circero. Riv. Anthropol. 35, 401–408.

Shea, B.T., 1985. Bivariate and multivariate growth allometry: statistical and biological considerations. J. Zool. Lond. (A) 206, 367–390.

Sládek, V., Šefčáková, A., Brůžek, J., 2001. Sex dimorphism among the early Upper Paleolithic hominids from Central Europe: cranial and pelvic metric variation. J. Hum. Evol. 43, A23.

Smith, F.H., 1983. Behavioral interpretations of changes in craniofacial morphology across the archaic/modern *Homo sapiens* transition. In: Trinkaus, E. (Ed.), The Mousterian Legacy. BAR S164, Oxford, pp. 137–209.

Smith, F.H., 2001. The Neandertals: evolutionary dead ends or ancestors of modern people? J. Anthropol. Res. 47, 219–238.

Smith, F.H., Falsetti, A.B., Donnelly, S.M., 1989. Modern human origins. Yearb. Phys. Anthropol. 32, 35–68.

Sohn, S., Wolpoff, M.H., 1993. Zuttiyeh face: a view from the east. Am. J. Phys. Anthropol. 91, 325–347.

Sokal, R.R., Rohlf, F.J., 1981. Biometry, second ed. W.H. Freeman and Co, San Francisco.

Sollas, W.J., 1908. On the cranial and facial characters of the Neandertal race. Phil. Trans. R. Soc. London. 199, 281–339.

Stewart, T.D., 1977. The Neanderthal skeletal remains from Shanidar Cave, Iraq: a summary of findings to date. Proc. Am. Philos. Soc. 121, 121–165.

Steyn, M., Pretorius, E., Hutten, L., 2004. Geometric morphometric analysis of the greater sciatic notch in South Africans. Homo 54, 197–206.

Strand Viðarsdóttir, U., O'Higgins, P., Stringer, C.B., 2002. A geometric morphometric study of regional differences in the growth of the modern human facial skeleton. J. Anat. 201, 211–229.

Stringer, C.B., 1985. Middle Pleistocene hominid variability and the origin of late Pleistocene humans. In: Delson, E. (Ed.), Ancestors: The Hard Evidence. Alan R. Liss, New York, pp. 289–295.

Stringer, C.B., Hublin, J.J., Vandermeersch, B., 1984. The origin of anatomically modern humans in Western Europe. In: Smith, F.H., Spencer, F. (Eds.), The Origins of Modern Humans: A World Survey of the Fossil Evidence. Alan R. Liss, New York, pp. 51–135.

Tattersall, I., Schwartz, J.H., 2006. The distinctiveness and systematic context of *Homo neanderthalensis*. In: Harvati, K., Harrison, T. (Eds.), Neanderthals Revisted: New Approaches and Perspectives. Springer, Dordrecht, pp. 9–22.

Terhune, C.E., Kimbel, W.H., Lockwood, C.A., 2007. Variation and diversity in *Homo erectus*: a 3D geometric morphometric analysis of the temporal bone. J. Hum. Evol. 53, 41–60.

Thorne, A.G., 1976. Morphological contrasts in Pleistocene Australians. In: Kirk, R.L., Thorne, A.G. (Eds.), The Origin of the Australians. Humanities Press, New Jersey, pp. 95–112.

Trinkaus, E., 1987. The Neandertal face: evolutionary and functional perspectives on a recent hominid face. J. Hum. Evol. 16, 429–443.

Trinkaus, E., 2003. Neandertal faces were not long; modern human faces are short. Proc. Natl. Acad. Sci. 100, 8142–8145.

Trinkaus, E., 2006. Modern human versus Neandertal evolutionary distinctiveness. Curr. Anthropol. 47, 597–620.

Wang, Q., Tobias, P.V., 2000. Review of the phylogenetic position of Chinese *Homo erectus* in light of midfacial morphology. Acta. Anthropol. Sinica 19, 23–33.

Weidenreich, F., 1943. The Skull of *Sinanthropus pekinensis*: A Comparative Study of a Primitive Hominid Skull. In: Palaeont. Sin, vol. 10. Geological Survey of China, Beijing.
White, T.D., 2000. Human Osteology, second ed. Academic Press, San Diego.
Williams, F.L., Krovitz, G.E., 2004. Ontogenetic migration of the mental foramen in Neandertals and modern humans. J. Hum. Evol. 47, 199–219.
Wolpoff, M.H., 1999. Paleoanthropology, second ed. McGraw-Hill, Boston.
Wolpoff, M.H., Smith, F.H., Malez, M., Radovčić, J., Rukavina, D., 1981. Upper Pleistocene human remains from Vindija Cave, Croatia, Yugoslavia. Am. J. Phys. Anthropol. 54, 499–545.
Wu, L., Zhang, Y., Wu, X., 2005. Middle Pleistocene human cranium from Tangshan (Nanjing), Southeast China: a new reconstruction and comparisons with *Homo erectus* from Eurasia and Africa. J. Hum. Evol. 127, 253–262.
Zollikofer, C.P.E., Ponce de Leon, M.S., 2004. Kinematics of cranial ontogeny: heterotopy, heterochrony, and geometric morphometric analysis of growth models. J. Exp. Zool. B. Mol. Dev. Evol. 302B, 322–340.
Zollikofer, C.P.E., Ponce de León, M.S., 2006. Cranial growth models: heterochrony, heterotropy, and the kinematics of ontogeny. In: Harvati, K., Harrison, T. (Eds.), Neanderthals Revisited: New Approaches and Perspectives. Springer, Dordrecht, pp. 89–112.